

Bayesian Nowcasting with Laplacian-P-Splines

Bryan Sumalinab, Oswaldo Gressani, Niel Hens & Christel Faes

To cite this article: Bryan Sumalinab, Oswaldo Gressani, Niel Hens & Christel Faes (2025) Bayesian Nowcasting with Laplacian-P-Splines, Journal of Computational and Graphical Statistics, 34:2, 718-728, DOI: [10.1080/10618600.2024.2395414](https://doi.org/10.1080/10618600.2024.2395414)

To link to this article: <https://doi.org/10.1080/10618600.2024.2395414>



© 2024 The Author(s). Published with license by Taylor & Francis Group, LLC.



[View supplementary material](#)



Published online: 08 Oct 2024.



[Submit your article to this journal](#)



Article views: 973



[View related articles](#)



[View Crossmark data](#)

Bayesian Nowcasting with Laplacian-P-Splines

Bryan Sumalinab^{a,b} , Oswaldo Gressani^a, Niel Hens^{a,c}, and Christel Faes^a

^aInteruniversity Institute for Biostatistics and Statistical Bioinformatics (I-BioStat), Data Science Institute (DSI), Hasselt University, Hasselt, Belgium; ^bDepartment of Mathematics and Statistics, College of Science and Mathematics, Mindanao State University - Iligan Institute of Technology, Iligan City, Philippines; ^cCentre for Health Economic Research and Modelling Infectious Diseases (CHERMID), Vaccine & Infectious Disease Institute, Antwerp University, Antwerp, Belgium

ABSTRACT

During an epidemic, the daily number of reported infected cases, deaths or hospitalizations is often lower than the actual number due to reporting delays. Nowcasting aims to estimate the cases that have not yet been reported and combine it with the already reported cases to obtain an estimate of the daily cases. In this article, we present a fast and flexible Bayesian approach for nowcasting by combining P-splines and Laplace approximations. Laplacian-P-splines provide a flexible framework for nowcasting that is computationally less demanding as compared to traditional Markov chain Monte Carlo techniques. The proposed approach also permits to naturally quantify the prediction uncertainty. Model performance is assessed through simulations and the nowcasting method is applied to COVID-19 mortality and incidence cases in Belgium. Supplementary materials for this article are available online.

ARTICLE HISTORY

Received July 2023
Accepted June 2024

KEYWORDS

Bivariate P-splines; COVID-19; Epidemic; Reporting delay



1. Introduction


Nowcasting is a term used for estimating the occurred-but-not-yet-reported-events (Donker et al. 2011; Van de Kastele, Eilers, and Wallinga 2019). In epidemiology, real-time updates of new symptomatic/infected individuals are helpful to assess the present situation and provide recommendations for rapid planning and for implementing essential measures to contain an epidemic outbreak. The exact number of new daily cases is frequently subject to reporting delays, resulting in underreporting of the real number of infected individuals for that day. Failing to account for the reporting delays will lead to possibly biased predictions that might have an effect on policy making (Gutierrez, Rubli, and Tavares 2020). The main goal of nowcasting is to estimate the actual number of new cases by combining the (predicted) not-yet-reported-cases with the already reported cases.

Lawless (1994), De Angelis and Gilks (1994), and Lindsey (1996) are among the first to establish a statistical modeling framework for this type of problem. In disease surveillance, Höhle and an der Heiden (2014) apply nowcasting to the outbreak of Shiga toxin-producing *Escherichia coli* in Germany and also to the SARS-CoV-2 outbreak (Glöckner, Krause, and Höhle 2020; Günther et al. 2021). Their approach is formulated within a hierarchical Bayesian framework and consists in estimating the epidemic curve by using a quadratic spline based on a truncated power basis function and to approximate the time-varying reporting delay distribution by a discrete time survival model. Van de Kastele, Eilers, and Wallinga (2019) point out

that a potential drawback of such a method is the long computation time required by the Markov chain Monte Carlo (MCMC) algorithm and therefore propose an alternative fast and flexible modelling strategy based on bivariate P-splines. P-splines (Eilers and Marx 1996) provide a flexible smoothing tool to describe trends in data. It introduces a penalty parameter that controls the roughness of the fit and counterbalances the flexibility of a rich B-spline basis. The relatively simple structure of the penalty matrix and the natural extension to a Bayesian framework (Lang and Brezger 2004) are two attractive features of the P-splines smoother. Based on the approach of Van de Kastele, Eilers, and Wallinga (2019), the number of cases are structured in a two-dimensional table (with calendar time as the first dimension and delay time as the second dimension), yielding the data matrix used as an input in the model. The reporting intensity is assumed to be a smooth surface and is modeled using two-dimensional P-splines.

In this article, we build upon the work of Van de Kastele, Eilers, and Wallinga (2019) and propose a new nowcasting methodology based on Laplacian-P-splines (LPS) in a fully Bayesian framework. A key advantage of working with the Bayesian paradigm is that it permits to naturally characterize the predictive distribution and quantify the uncertainty associated with the predictions. The Laplace approximation uses a second-order Taylor expansion to approximate the posterior distribution of the regression parameters by a Gaussian density. It is a sampling-free method with the major advantage of faster computational time as compared to MCMC approaches; the

CONTACT Bryan Sumalinab  bryan.sumalinab@uhasselt.be  Interuniversity Institute for Biostatistics and Statistical Bioinformatics (I-BioStat), Data Science Institute (DSI), Hasselt University, Agoralaan Gebouw D, 3590 Diepenbeek, Belgium.

 Supplementary materials for this article are available online. Please go to www.tandfonline.com/r/JCGS.

© 2024 The Author(s). Published with license by Taylor & Francis Group, LLC.

This is an Open Access article distributed under the terms of the Creative Commons Attribution License (<http://creativecommons.org/licenses/by/4.0/>), which permits unrestricted use, distribution, and reproduction in any medium, provided the original work is properly cited. The terms on which this article has been published allow the posting of the Accepted Manuscript in a repository by the author(s) or with their consent.

gold benchmark to explore posterior distributions. Therefore, the flexibility of P-splines smoothers and the computational benefit of Laplace approximations are interesting features to be considered in a Bayesian nowcasting model. Laplacian-P-splines already proved to be useful in survival models (Gressani and Lambert 2018; Gressani, Faes, and Hens 2022a), generalized additive models (Gressani and Lambert 2021) and also in epidemic models for estimating the time-varying reproduction number (Gressani et al. 2022b; Gressani, Faes, and Hens 2023; Sumalinab et al. 2024). We build on the work of Gressani and Lambert (2021) and extend the Laplacian-P-splines methodology to nowcasting, thereby providing a fast and flexible Bayesian model alternative to Van de Kastele, Eilers, and Wallinga (2019). To evaluate the (predictive) performance of our method, a simulation study is implemented and several performance measures are reported such as the (relative) bias, prediction interval coverage, and prediction interval width. Finally, our method is applied to COVID-19 mortality and incidence data in Belgium for the year 2021 and 2022, respectively. R code used for the simulation study is available on GitHub (<https://github.com/bryansumalinab/Laplacian-P-spline-nowcasting.git>).

2. Methodology

2.1. Bayesian Model Formulation

Let $y_{t,d}$ denote the number of cases that occurred at time $t = 1, 2, \dots, T$ (corresponding to the calendar day) and are reported with a delay of $d = 0, 1, 2, \dots, D$ days. The information on cases can be summarized in matrix form:

$$Y = \begin{bmatrix} y_{1,0} & y_{1,1} & y_{1,2} & \dots & y_{1,D} \\ y_{2,0} & y_{2,1} & y_{2,2} & \dots & y_{2,D} \\ \vdots & \vdots & \vdots & \dots & \vdots \\ y_{T-(D-1),0} & y_{T-(D-1),1} & y_{T-(D-1),2} & \dots & y_{T-(D-1),D} \\ \vdots & \vdots & \vdots & \dots & \vdots \\ y_{T-1,0} & y_{T-1,1} & y_{T-1,2} & \dots & y_{T-1,D} \\ y_{T,0} & y_{T,1} & y_{T,2} & \dots & y_{T,D} \end{bmatrix},$$

with cases that have not yet been reported (at time T) highlighted in bold. The not-yet-reported cases correspond to (t, d) combinations satisfying $t > T - d$. The main objective is to predict the total number of cases, $y_t = \sum_{d=0}^D y_{t,d}$, for $t = T - (D - 1), \dots, T$ for which the nowcasted and already reported cases can be combined.

Let $\mathcal{D} := \mathbf{y} = (y_1, y_2, \dots, y_n)^\top$ denote the observed number of cases by stacking the columns of matrix Y for the reported cases, where each entry corresponds to each (t, d) combination of reported cases $y_{t,d}$. The model assumes that the number of cases either follows a Poisson or a negative binomial (NB) distribution, that is $y_{t,d} \sim \text{Poisson}(\mu_{t,d})$ or $y_{t,d} \sim \text{NB}(\mu_{t,d}, \phi)$ with mean $\mu_{t,d} > 0$. For the negative binomial, $\phi > 0$ is an overdispersion parameter and the variance is $\mathbb{V}(y_{t,d}) = \mu_{t,d} + \mu_{t,d}^2/\phi$. Following Van de Kastele, Eilers, and Wallinga (2019), the (log) mean number of cases is modeled with two-dimensional B-splines:

$$\log(\mu_{t,d}) = \beta_0 + \sum_{j=1}^{K_T} \sum_{k=1}^{K_D} \theta_{j,k} b_j(t) b_k(d) + \sum_{l=1}^p \beta_l z_l(t, d), \quad (2.1)$$

where β_0 is the intercept; $b_j(\cdot)$ and $b_k(\cdot)$ are univariate B-splines basis functions specified in the time and delay dimensions, respectively; and $z_l(t, d)$ represents additional covariates with regression coefficients β_l . In matrix notation:

$$\log(\boldsymbol{\mu}) = B\boldsymbol{\theta} + Z\boldsymbol{\beta}, \quad (2.2)$$

where matrices B and Z correspond to the basis functions and covariates, respectively, and vectors $\boldsymbol{\theta}$ and $\boldsymbol{\beta}$ are the associated parameters to be estimated (details in supplementary material S1).

Following the philosophy of Eilers and Marx (1996), we use a rich (cubic) B-splines basis and counterbalance the associated flexibility by imposing a discrete roughness penalty on contiguous B-spline coefficients. For two-dimensional P-splines, the penalty can be obtained based on row-wise (direction of calendar time) and column-wise (direction of reporting delay) differences for matrix $\Theta = (\theta_{j,k})$ with $j = 1, \dots, K_T$ and $k = 1, \dots, K_D$ as shown in supplementary material S1 (Durbán, Currie, and Eilers 2002; Fahrmeir et al. 2013). Let D_t^m and D_d^m denote the m th order row-wise and column-wise difference matrix (here $m = 2$) with dimensions $(K_T - m) \times K_T$ and $(K_D - m) \times K_D$, respectively. For ease of notation, let $D_t = D_t^m$ and $D_d = D_d^m$. The difference matrix for vector $\boldsymbol{\theta}$ can be obtained by expanding the difference matrix into $I_{K_D} \otimes D_t$ and $D_d \otimes I_{K_T}$, where \otimes denotes the Kronecker product. Using this notation, the row-wise and column-wise difference penalty can be written as

$$\begin{aligned} \|(I_{K_D} \otimes D_t)\boldsymbol{\theta}\|^2 &= \boldsymbol{\theta}^\top (I_{K_D} \otimes D_t)^\top (I_{K_D} \otimes D_t) \boldsymbol{\theta} \\ &= \boldsymbol{\theta}^\top (I_{K_D} \otimes D_t^\top D_t) \boldsymbol{\theta} \quad \text{and} \\ \|(D_d \otimes I_{K_T})\boldsymbol{\theta}\|^2 &= \boldsymbol{\theta}^\top (D_d \otimes I_{K_T})^\top (D_d \otimes I_{K_T}) \boldsymbol{\theta} \\ &= \boldsymbol{\theta}^\top (D_d^\top D_d \otimes I_{K_T}) \boldsymbol{\theta}. \end{aligned}$$

Let $\lambda_t > 0$ and $\lambda_d > 0$ denote the row-wise and column-wise penalty parameter, respectively. The penalty for the two-dimensional B-spline basis becomes:

$$\begin{aligned} &\lambda_t \boldsymbol{\theta}^\top (I_{K_D} \otimes D_t^\top D_t) \boldsymbol{\theta} + \lambda_d \boldsymbol{\theta}^\top (D_d^\top D_d \otimes I_{K_T}) \boldsymbol{\theta} \\ &= \boldsymbol{\theta}^\top \left(\lambda_t (I_{K_D} \otimes D_t^\top D_t) + \lambda_d (D_d^\top D_d \otimes I_{K_T}) \right) \boldsymbol{\theta}. \end{aligned}$$

Let us define the penalty matrices $P_t = D_t^\top D_t + \delta I_{K_T}$ and $P_d = D_d^\top D_d + \delta I_{K_D}$, where δ is a small number (say $\delta = 10^{-12}$), to ensure that the penalty matrices are full rank and thus invertible. Following Lang and Brezger (2004), the penalty can be translated in a Bayesian framework by specifying a Gaussian prior $(\boldsymbol{\theta} | \boldsymbol{\lambda}) \sim \mathcal{N}_{\dim(\boldsymbol{\theta})}(\mathbf{0}, \mathcal{P}^{-1}(\boldsymbol{\lambda}))$, where $\boldsymbol{\lambda} = (\lambda_t, \lambda_d)^\top$ is the penalty vector and $\mathcal{P}(\boldsymbol{\lambda}) = \lambda_t (I_{K_D} \otimes P_t) + \lambda_d (P_d \otimes I_{K_T})$ is the precision matrix. An uninformative Gaussian prior is assumed for $\boldsymbol{\beta}$, namely $\boldsymbol{\beta} \sim \mathcal{N}_{\dim(\boldsymbol{\beta})}(\mathbf{0}, V_\beta^{-1})$ with $V_\beta = \zeta I_{p+1}$ ($\zeta = 10^{-5}$). Denote by $X = (B, Z)$ the global design matrix, $\boldsymbol{\xi} = (\boldsymbol{\theta}^\top, \boldsymbol{\beta}^\top)^\top$ the latent parameter vector and $Q_\xi^\lambda = \text{blkdiag}(\mathcal{P}(\boldsymbol{\lambda}), V_\beta)$ the precision matrix for $\boldsymbol{\xi}$, where $\text{blkdiag}(\cdot)$ refers to a block diagonal matrix. From here, we focus on the negative binomial model for the number of cases. The Poisson model is described in supplementary material S4. The Bayesian model is summarized as follows:

$$(y_i|\xi) \sim \text{NB}(\mu_i, \phi) \text{ with } \log(\mu) = X\xi,$$

$$(\xi|\lambda) \sim \mathcal{N}_{\dim(\xi)}(\mathbf{0}, (Q_\xi^\lambda)^{-1}),$$

$$(\lambda_t|\delta_t) \sim \mathcal{G}\left(\frac{\nu}{2}, \frac{\nu\delta_t}{2}\right),$$

$$(\lambda_d|\delta_d) \sim \mathcal{G}\left(\frac{\nu}{2}, \frac{\nu\delta_d}{2}\right),$$

$$\delta_t \sim \mathcal{G}(a_\delta, b_\delta),$$

$$\delta_d \sim \mathcal{G}(a_\delta, b_\delta),$$

$$\phi \sim \mathcal{G}(a_\phi, b_\phi),$$

where $\mathcal{G}(a, b)$ denotes a Gamma distribution with mean a/b and variance a/b^2 . The prior specification on the penalty parameters follows from Jullion and Lambert (2007). They have shown that when hyperparameters a_δ, b_δ are chosen to be equal and small enough (say 10^{-5}), then the resulting fit is robust to the value of ν ($\nu = 3$ in this article). In addition, we impose an uninformative Gamma prior on the overdispersion parameter with $a_\phi = b_\phi = 10^{-5}$.

2.2. Laplace Approximation to the Conditional Posterior of ξ

The conditional posterior of the latent vector ξ is approximated by a Gaussian distribution via the Laplace approximation. The gradient and Hessian of the (log) conditional posterior are analytically derived and used in a Newton-Raphson algorithm to obtain the Gaussian approximation to the conditional posterior distribution of ξ .

For a negative binomial distributed y_i with mean $\mathbb{E}(y_i) = \mu_i$, the probability distribution can be written as an exponential dispersion family given by $p(y_i; \gamma_i, \phi) = \exp\left((y_i\gamma_i - b(\gamma_i))/a(\phi) + c(\gamma_i, \phi)\right)$, where $\gamma_i = \phi \log\left(\frac{\mu_i}{\mu_i + \phi}\right)$, $b(\gamma_i) = -\phi^2 \log\left(\frac{\phi}{\mu_i + \phi}\right)$, $c(\gamma_i, \phi) = \log\left(\frac{\Gamma(y_i + \phi)}{\Gamma(y_i + 1)\Gamma(\phi)}\right)$, $a(\phi) = \phi$, and $\Gamma(\cdot)$ is the gamma function. Thus, for fixed ϕ , a negative binomial regression model is a generalized linear model (GLM) where μ_i is linked to the linear predictor through the link function $g(\mu_i)$. Our setting uses a log-link function $g(\mu_i) = \log(\mu_i)$ and the log-likelihood is given by $\log \mathcal{L}(\xi, \phi; \mathcal{D}) = \sum_{i=1}^n ((y_i\gamma_i - b(\gamma_i))/a(\phi) + c(\gamma_i, \phi))$. It can be shown that for a negative binomial model, the gradient and Hessian are:

$$\nabla_\xi \log \mathcal{L}(\xi, \phi; \mathcal{D}) = X^\top W D (\mathbf{y} - \mu) \quad \text{and}$$

$$\nabla_\xi^2 \log \mathcal{L}(\xi, \phi; \mathcal{D}) = X^\top M V X - X^\top W X,$$

where $W = \text{diag}(w_1, \dots, w_n)$, $w_i = [\nabla(y_i)(g'(\mu_i))^2]^{-1}$, $D = \text{diag}(g'(\mu_1), \dots, g'(\mu_n))$, $V = \text{diag}(v_1, v_2, \dots, v_n)$, $v_i = g'(\mu_i)^{-1} \left(\nabla(y_i)^{-1} (\partial(g'(\mu_i)^{-1})/\partial\mu_i) + g'(\mu_i)^{-1} (\partial(\nabla(y_i)^{-1})/\partial\mu_i) \right)$ and $M = \text{diag}(y_1 - \mu_1, \dots, y_n - \mu_n)$. Further details are provided in supplementary material S2.

Using Bayes' rule, the posterior of ξ conditional on the penalty vector λ and overdispersion parameter ϕ is:

$$p(\xi|\lambda, \phi, \mathcal{D}) \propto \mathcal{L}(\xi, \phi; \mathcal{D}) p(\xi|\lambda) \\ \propto \exp\left(\frac{1}{\phi} \sum_{i=1}^n (y_i\gamma_i - b(\gamma_i)) - \frac{1}{2} \xi^\top Q_\xi^\lambda \xi\right).$$

The gradient and Hessian for the log-conditional posterior of ξ are:

$$\nabla_\xi \log p(\xi|\lambda, \phi, \mathcal{D}) = X^\top W D (\mathbf{y} - \mu) - Q_\xi^\lambda \xi,$$

$$\nabla_\xi^2 \log p(\xi|\lambda, \phi, \mathcal{D}) = X^\top M V X - X^\top W X - Q_\xi^\lambda.$$

The above gradient and Hessian are used in a Newton-Raphson algorithm to approximate the mode of the conditional posterior of ξ . After convergence, the Laplace approximation to the conditional posterior of ξ is a multivariate Gaussian density denoted by $\tilde{p}_G(\xi|\lambda, \phi, \mathcal{D}) = \mathcal{N}_{\dim(\xi)}(\hat{\xi}_\lambda, \hat{\Sigma}_\lambda)$ with mean and covariance matrix obtained from the Newton-Raphson algorithm. There are situations where the Laplace approximation provides a poor summary of the target posterior distribution, for example in scenarios of sparse likelihoods or low counts. In such scenarios, the resulting posterior distribution may exhibit skewness and Lambert and Gressani (2023) propose an approach to address this issue in a Laplacian-P-splines context.

2.3. Optimization of Hyperparameters and Overdispersion Parameter

In this section, we derive the (approximate) posterior distribution of the hyperparameters $\lambda = (\lambda_t, \lambda_d)^\top$ and $\delta = (\delta_t, \delta_d)^\top$, and overdispersion parameter ϕ . Let $\eta = (\lambda_t, \lambda_d, \delta_t, \delta_d)^\top$ denote the vector of hyperparameters. Using Bayes' theorem, the joint posterior of η and ϕ is

$$p(\eta, \phi|\mathcal{D}) \propto \frac{\mathcal{L}(\xi, \phi; \mathcal{D}) p(\xi|\lambda) p(\lambda|\delta) p(\delta) p(\phi)}{p(\xi|\lambda, \phi, \mathcal{D})}.$$

Following Rue, Martino, and Chopin (2009), the above posterior can be approximated by replacing $p(\xi|\lambda, \phi, \mathcal{D})$ with $\tilde{p}_G(\xi|\lambda, \phi, \mathcal{D})$ obtained in Section 2.2 and by evaluating the latent vector at $\hat{\xi}_\lambda$. Note that $\gamma_i = \mathbf{x}_i^\top \xi$, where \mathbf{x}_i^\top corresponds to the i th row of the design matrix X . Also, the determinant $|Q_\xi^\lambda|$ in $p(\xi|\lambda)$ is $|Q_\xi^\lambda| \propto |\mathcal{P}(\lambda)|$. Hence, the approximated joint posterior of η and ϕ is

$$\tilde{p}(\eta, \phi|\mathcal{D}) \propto \frac{\mathcal{L}(\xi, \phi; \mathcal{D}) p(\xi|\lambda) p(\lambda|\delta) p(\delta) p(\phi)}{p(\xi|\lambda, \phi, \mathcal{D})} \Big|_{\xi=\hat{\xi}_\lambda} \\ \propto \exp\left(\sum_{i=1}^n \left((y_i \mathbf{x}_i^\top \hat{\xi}_\lambda - b(\mathbf{x}_i^\top \hat{\xi}_\lambda)) / \phi \right. \right. \\ \left. \left. + \log(\Gamma(y_i + \phi)) - \log \Gamma(\phi) \right) \right) \\ \times |\mathcal{P}(\lambda)|^{\frac{1}{2}} \exp\left(-\frac{1}{2} \hat{\xi}_\lambda^\top Q_\xi^\lambda \hat{\xi}_\lambda\right) \\ \times (\lambda_t \lambda_d)^{(\frac{\nu}{2}-1)} \delta_t^{(\frac{\nu}{2}+a_\delta-1)} \exp\left(-\delta_t(b_\delta + \frac{\nu}{2} \lambda_t)\right)$$

$$\begin{aligned} & \times \delta_d^{(\frac{\nu}{2}+a_\delta-1)} \exp\left(-\delta_d(b_\delta + \frac{\nu}{2}\lambda_d)\right) \\ & \times \phi^{(a_\phi-1)} \exp(-b_\phi\phi) |\widehat{\Sigma}_\lambda|^{\frac{1}{2}}. \end{aligned}$$

Integrating out the hyperparameters δ_t and δ_d from $\tilde{p}(\eta, \phi | \mathcal{D})$, we obtain the joint marginal posterior of λ and ϕ :

$$\begin{aligned} \tilde{p}(\lambda, \phi | \mathcal{D}) &= \int_0^\infty \int_0^\infty \tilde{p}(\eta, \phi | \mathcal{D}) d\delta_t d\delta_d \\ &\propto \exp\left(\sum_{i=1}^n \left((y_i \mathbf{x}_i^\top \widehat{\xi}_\lambda - b(\mathbf{x}_i^\top \widehat{\xi}_\lambda)) / \phi \right. \right. \\ &\quad \left. \left. + \log(\Gamma(y_i + \phi)) - \log \Gamma(\phi)\right)\right) \\ &\quad \times |\mathcal{P}(\lambda)|^{\frac{1}{2}} \exp\left(-\frac{1}{2} \widehat{\xi}_\lambda^\top Q_\xi^\lambda \widehat{\xi}_\lambda\right) \phi^{(a_\phi-1)} \\ &\quad \times \exp(-b_\phi\phi) |\widehat{\Sigma}_\lambda|^{\frac{1}{2}} \\ &\quad \times (\lambda_t \lambda_d)^{(\frac{\nu}{2}-1)} \left(b_\delta + \frac{\nu}{2}\lambda_t\right) \left(b_\delta + \frac{\nu}{2}\lambda_d\right)^{-\left(\frac{\nu}{2}+a_\delta\right)}. \end{aligned}$$

To ensure numerical stability, the penalty vector is log transformed $\mathbf{v} = (v_t, v_d)^\top = (\log(\lambda_t), \log(\lambda_d))^\top$ and so is the overdispersion parameter $v_\phi = \log(\phi)$. The joint log-posterior of \mathbf{v} and v_ϕ is then given by:

$$\begin{aligned} \log \tilde{p}(\mathbf{v}, v_\phi | \mathcal{D}) &\doteq \sum_{i=1}^n \left((y_i \mathbf{x}_i^\top \widehat{\xi}_\mathbf{v} - b(\mathbf{x}_i^\top \widehat{\xi}_\mathbf{v})) / \exp(v_\phi) \right. \\ &\quad \left. + \log(\Gamma(y_i + \exp(v_\phi))) - \log \Gamma(\exp(v_\phi)) \right) \\ &\quad + \frac{1}{2} \log |P(\mathbf{v})| - \frac{1}{2} \widehat{\xi}_\mathbf{v}^\top Q_\xi^\mathbf{v} \widehat{\xi}_\mathbf{v} \\ &\quad + a_\phi v_\phi - b_\phi e^{v_\phi} + \frac{1}{2} \log |\widehat{\Sigma}_\mathbf{v}| \\ &\quad + \frac{\nu}{2} (v_d + v_t) - \left(\frac{\nu}{2} + a_\delta\right) \\ &\quad \left(\log(b_\delta + \frac{\nu}{2} \exp(v_d)) + \log(b_\delta + \frac{\nu}{2} \exp(v_t)) \right), \end{aligned}$$

where \doteq denotes equality up to an additive constant. Finally, $\log \tilde{p}(\mathbf{v}, v_\phi | \mathcal{D})$ is maximized using the *optim()* function in R to obtain the posterior mode as a point estimate for \mathbf{v} and v_ϕ .

2.4. Nowcasting and Prediction Interval

To obtain the mean nowcast estimate with the prediction interval, note that $\log(\mu_i) = \mathbf{x}_i^\top \xi$ or equivalently $\log(\mu_{t,d}) = \mathbf{x}_{t,d}^\top \xi$, where $\tilde{p}_G(\xi | \mathbf{v}, \mathcal{D}) = \mathcal{N}_{\dim(\xi)}(\widehat{\xi}_\mathbf{v}, \widehat{\Sigma}_\mathbf{v})$. Thus, $\tilde{p}(\log(\mu_{t,d}) | \mathbf{v}, \mathcal{D}) = \mathcal{N}_1(\mathbf{x}_{t,d}^\top \widehat{\xi}_\mathbf{v}, \mathbf{x}_{t,d}^\top \widehat{\Sigma}_\mathbf{v} \mathbf{x}_{t,d})$. The mean estimate for the not-yet-reported cases is calculated as $\widehat{\mu}_{t,d} = \exp(\mathbf{x}_{t,d}^\top \widehat{\xi}_\mathbf{v})$ for all (t, d) combinations with $t > T - d$. Next, the estimate for the total number of cases for each t is obtained by summing the already reported cases and the mean estimate for the not-yet-reported cases, that is

$$\widehat{\mu}_t = \sum_{\{d: t \leq T-d\}} y_{t,d} + \sum_{\{d: t > T-d\}} \widehat{\mu}_{t,d}.$$

The prediction interval for the nowcast values is obtained by sampling from the posterior predictive distribution of the log-mean number of cases through the following steps:

1. For each (t, d) combination with $t > T - d$ (corresponding to the not-yet-reported cases), generate 1000 random samples $(\widehat{\mathbf{y}}_{t,d})$ from a Gaussian distribution with mean $\mathbf{x}_{t,d}^\top \widehat{\xi}_\mathbf{v}$ and variance $\mathbf{x}_{t,d}^\top \widehat{\Sigma}_\mathbf{v} \mathbf{x}_{t,d}$.
2. Exponentiate the sampled values from the previous step to obtain the (estimated) average reporting intensities $\widehat{\mu}_{t,d} = \exp(\widehat{\mathbf{y}}_{t,d})$.
3. Compute the average prediction for the not-yet-reported cases for each t , that is, compute $\widehat{\mu}_t = \sum_d \widehat{\mu}_{t,d}$ for $t > T - d$.
4. For each t , sample $\widehat{\mathbf{y}}_t$ containing 1000 values from the $\text{NB}(\widehat{\mu}_t, \exp(\widehat{v}_\phi))$ distribution.
5. Finally, compute the quantiles of the sampled values $\widehat{\mathbf{y}}_t$ corresponding to the desired prediction interval.

2.5. Delay Distribution

To obtain the smooth estimate of the delay distribution, only the first term on the right hand side of (2.2) is used (excluding day of the week effects), as explained in the paper of Van de Kasstele, Eilers, and Wallinga (2019). Specifically, the procedure to compute the delay distribution is as follows:

1. Compute the contribution of the smoothing term in (2.2) to the reporting intensity for all (t, d) combinations: $\mu^{\text{smooth}} = \exp(B\theta)$.
2. Arrange μ^{smooth} into a $T \times (D + 1)$ matrix with entries $\mu_{t,d}^{\text{smooth}}$.
3. For each $t = 1, \dots, T$, compute the reporting delay distribution given by: $\widehat{f}_t(d) = \mu_{t,d}^{\text{smooth}} / \sum_{d=0}^D \mu_{t,d}^{\text{smooth}}$.

3. Simulations

A simulation study is implemented in order to evaluate the predictive performance of the proposed method. The procedure to perform the simulations is as follows:

1. Consider a function $f(t)$ that represents the mean epidemic curve of all cases such that $\mu(t) = \exp(f(t))$ for $t = 1, \dots, T$.
2. For each t , generate a random sample y_t from a negative binomial distribution with mean $\mu(t)$ and fixed overdispersion parameter (here $\phi = 10$).
3. To account for possible delays $d = 0, 1, 2, \dots, D$, generate samples from a multinomial distribution with probabilities $p_0, p_1, p_2, \dots, p_D$ such that $\sum_{d=0}^D p_d = 1$:
 $(y_{t,0}, y_{t,1}, y_{t,2}, \dots, y_{t,D}) \sim \text{Multinomial}(y_t, p_0, p_1, p_2, \dots, p_D)$.
 This sample represents the reported number of cases for each (t, d) combination.
4. Steps 1–3 are repeated 500 times to generate 500 possible realizations.

For the epidemic curve, the following two functions inspired from the paper of Noufaily et al. (2016) are used:

$$\begin{aligned} f(t) &= \theta_1 + \theta_2 \sin\left(\frac{2\pi t}{150}\right), \\ h(t) &= \theta_1 + \theta_2 \sin\left(\frac{2\pi t}{150}\right) + \theta_3 \sqrt{t}, \end{aligned}$$

for $t = 1, \dots, 365$ so that a yearly time window (365 days) is assumed in the simulations. In terms of delay probabilities,

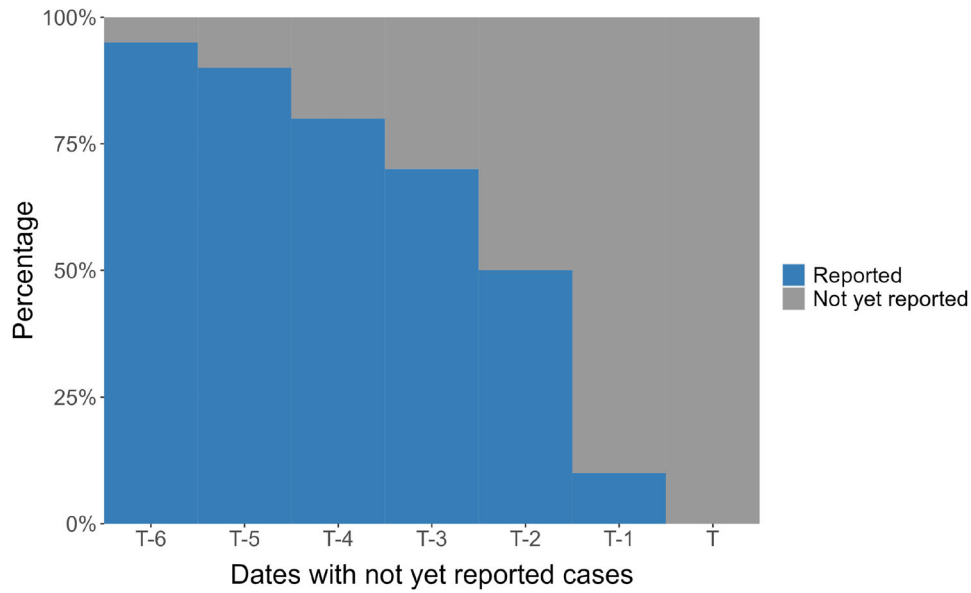


Figure 1. Illustration of the delay probabilities considered in the simulations.

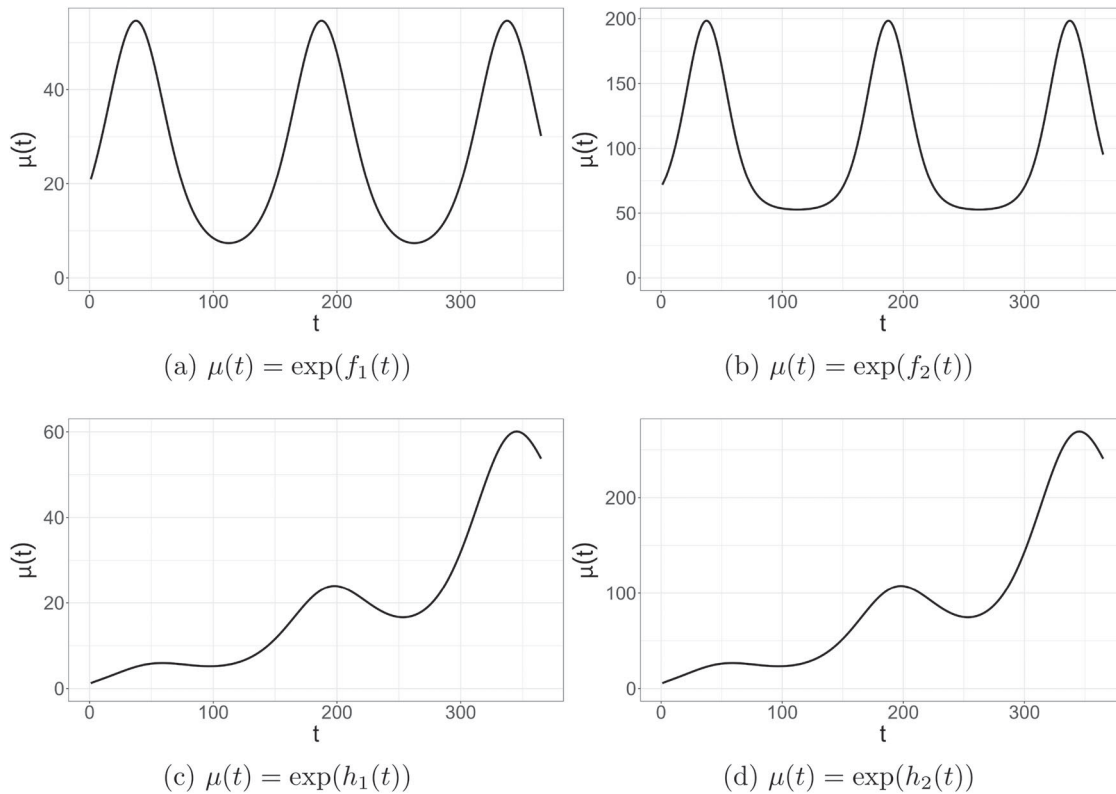


Figure 2. Mean epidemic curves considered in the simulations.

we consider a maximum delay of $D = 7$ days with probabilities $(p_0, p_1, p_2, \dots, p_7) = (0.0, 0.1, 0.4, 0.2, 0.1, 0.1, 0.05, 0.05)$, as illustrated in Figure 1. This means that 5% of the cases that occurred at time $T - 6$ have a delay of 7 days (with probability $p_7 = 0.05$) and still need to be reported, or equivalently, 95% of the cases that occurred at time $T - 6$ have already been reported. For cases that occurred at time $T - 5$, only 90% of these cases have been reported, as cases with delays of 6 and 7 days are yet to be reported. For those cases that occurred on the nowcast day (time T), no cases are reported and the delay is 100%.

Two scenarios are considered for $f(t)$: (i) the first has a small number of cases with values of $\theta_1 = 3$ and $\theta_2 = 1$; (ii) the second scenario has a relatively large number of cases with $\theta_1 = 3$ and $\theta_2 = 2$ and an additional factor of 50 is added to the mean function such that $\mu(t) = 50 + \exp(f(t))$. These scenarios are denoted by $f_1(t)$ and $f_2(t)$, respectively. Similarly, two scenarios are also considered for the second function $h(t)$: (i) the first scenario has values $\theta_1 = 0$, $\theta_2 = 0.4$, and $\theta_3 = 0.2$; (ii) the second scenario has values $\theta_1 = 1.5$, $\theta_2 = 0.4$ and $\theta_3 = 0.2$. We denote these functions by $h_1(t)$ and $h_2(t)$, respectively. The first

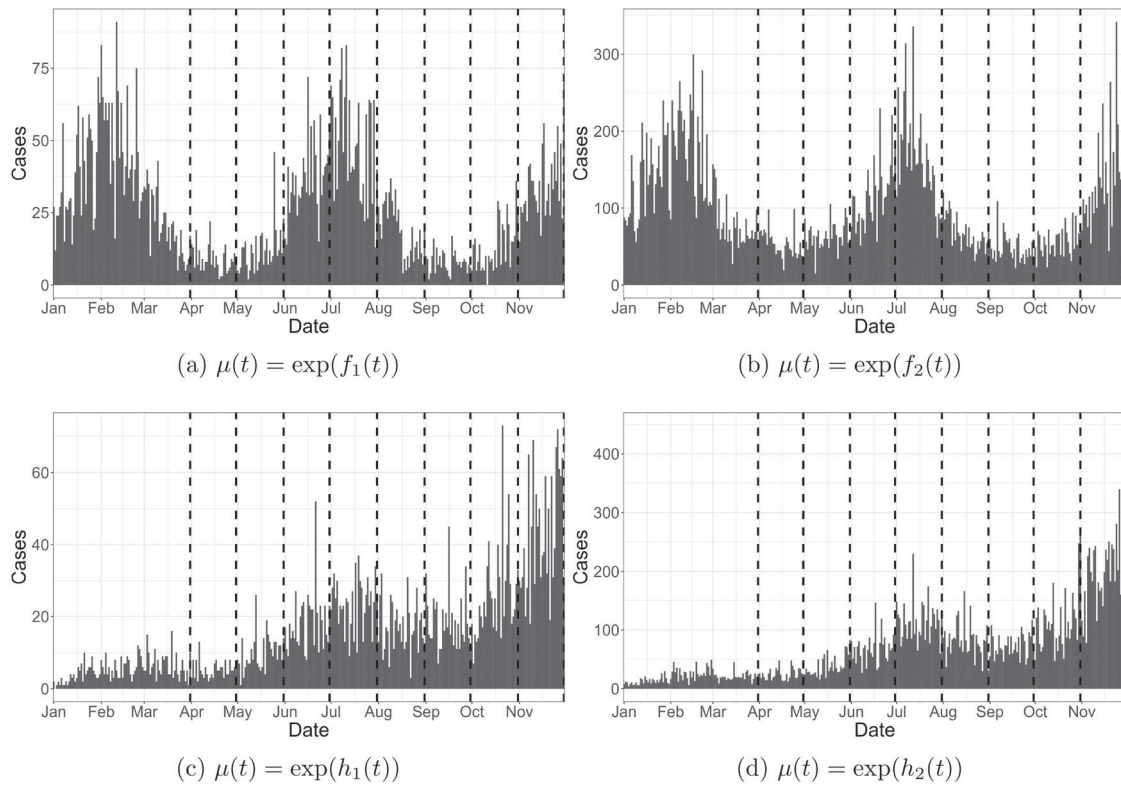


Figure 3. Simulated cases for different epidemic curves. The dashed vertical lines correspond to different nowcast dates.

Table 1. Performance on the nowcast date for function $f_1(t)$: **LPS-NB**—LPS model with a negative binomial distribution for the number of cases; **LPS-P**—LPS with a Poisson distribution for the number of cases; **VDK**—Methodology of Van de Kasstelee, Eilers, and Wallinga (2019).

| | 95% PI coverage | | | PI width | | | Bias (μ) | | | % Bias (μ) | | |
|-------|-----------------|-------|-------|----------|-------|-------|----------------|-------|------|------------------|-------|------|
| | LPS-NB | LPS-P | VDK | LPS-NB | LPS-P | VDK | LPS-NB | LPS-P | VDK | LPS-NB | LPS-P | VDK |
| March | 95.8 | 78.6 | 99.8 | 48.9 | 32.7 | 74.9 | 1.7 | 3.1 | 4.0 | 32.1 | 47.7 | 70.2 |
| Apr | 97.6 | 86.0 | 99.2 | 20.7 | 15.6 | 28.2 | −0.4 | 0.4 | −1.6 | 23.9 | 30.9 | 32.3 |
| May | 96.6 | 73.0 | 100.0 | 41.5 | 25.2 | 73.7 | −1.9 | 1.8 | −3.0 | 19.3 | 26.4 | 27.9 |
| June | 96.0 | 54.0 | 99.6 | 98.6 | 42.2 | 226.5 | −0.1 | 9.3 | 15.3 | 14.7 | 27.7 | 35.3 |
| July | 96.0 | 60.6 | 98.4 | 63.5 | 29.2 | 192.2 | 1.1 | 5.0 | 20.2 | 14.1 | 25.2 | 66.9 |
| Aug | 95.6 | 83.8 | 98.8 | 19.0 | 13.4 | 31.8 | −0.7 | 0.2 | −1.3 | 16.2 | 19.3 | 28.3 |
| Sept | 94.0 | 85.6 | 98.2 | 14.5 | 11.3 | 23.9 | −1.3 | −0.5 | −1.9 | 19.2 | 19.1 | 31.9 |
| Oct | 95.6 | 72.6 | 99.2 | 38.6 | 21.3 | 69.2 | −2.2 | 0.5 | −3.0 | 14.8 | 16.8 | 23.7 |
| Nov | 97.2 | 48.8 | 99.0 | 96.6 | 34.0 | 232.5 | 4.7 | 4.9 | 21.7 | 14.5 | 17.8 | 43.0 |

Table 2. Performance on the nowcast date for function $h_1(t)$: **LPS-NB**—LPS model with a negative binomial distribution for the number of cases; **LPS-P**—LPS with a Poisson distribution for the number of cases; **VDK**—Methodology of Van de Kasstelee, Eilers, and Wallinga (2019).

| | 95% PI coverage | | | PI width | | | Bias (μ) | | | % Bias (μ) | | |
|-------|-----------------|-------|------|----------|-------|-------|----------------|-------|------|------------------|-------|------|
| | LPS-NB | LPS-P | VDK | LPS-NB | LPS-P | VDK | LPS-NB | LPS-P | VDK | LPS-NB | LPS-P | VDK |
| March | 96.6 | 81.2 | 95.6 | 26.5 | 19.1 | 13.2 | 1.3 | 2.0 | −0.3 | 41.1 | 55.3 | 20.3 |
| Apr | 97.4 | 85.8 | 93.8 | 18.8 | 13.1 | 12.9 | 0.2 | 0.7 | −0.9 | 25.5 | 33.1 | 23.2 |
| May | 97.2 | 78.4 | 95.2 | 26.4 | 16.4 | 20.9 | −0.6 | 0.4 | −1.7 | 20.4 | 25.4 | 19.2 |
| June | 95.8 | 75.2 | 95.2 | 40.5 | 21.7 | 39.6 | −1.6 | 0.7 | −0.5 | 16.6 | 21.4 | 15.3 |
| July | 96.4 | 72.0 | 96.4 | 40.0 | 21.7 | 49.2 | −1.4 | 1.3 | 1.9 | 15.0 | 19.8 | 17.2 |
| Aug | 94.4 | 77.6 | 97.6 | 29.2 | 17.9 | 34.6 | −1.6 | 0.4 | −0.7 | 15.5 | 18.0 | 15.7 |
| Sept | 96.0 | 77.6 | 96.8 | 30.7 | 18.4 | 34.8 | −2.3 | −0.1 | −2.6 | 16.5 | 17.5 | 18.5 |
| Oct | 96.2 | 66.0 | 97.8 | 54.7 | 25.8 | 69.2 | −3.0 | 0.6 | −1.1 | 13.9 | 16.4 | 14.7 |
| Nov | 97.6 | 49.4 | 96.4 | 94.4 | 34.3 | 157.1 | 0.2 | 3.8 | 16.7 | 11.3 | 16.6 | 30.9 |

function is symmetric with three peaks as shown in Figure 2(a) and (b). On the other hand, the second function is not periodic as opposed to the first function (see Figure 2(c) and (d)). The plots for (one realization of) simulated cases based on these functions are shown in Figure 3 with (dashed) vertical lines corresponding to the different nowcast dates.

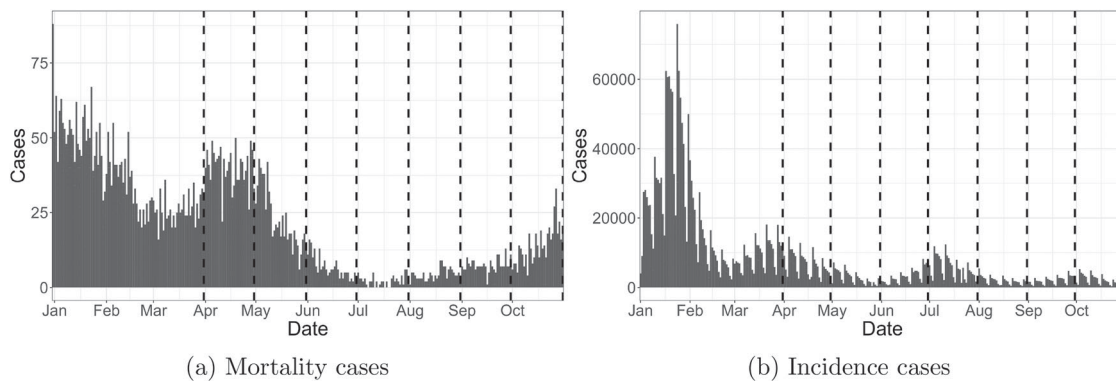
For each generated dataset, we fit the LPS-NB (negative binomial assumption) and LPS-P (Poisson assumption) models as well as the method proposed by Van de Kasstelee, Eilers, and Wallinga (2019) (VDK), and compute the following performance measures. The bias and relative bias (% bias) with respect to the true mean epidemic curve (μ) and the 95%

Table 3. Performance on the nowcast date for function $f_2(t)$: **LPS-NB**—LPS model with a negative binomial distribution for the number of cases; **LPS-P**—LPS with a Poisson distribution for the number of cases.

| | 95% PI coverage | | PI width | | Bias (μ) | | % Bias (μ) | |
|-------|-----------------|-------|----------|-------|----------------|-------|------------------|-------|
| | LPS-NB | LPS-P | LPS-NB | LPS-P | LPS-NB | LPS-P | LPS-NB | LPS-P |
| March | 96.8 | 49.4 | 296.2 | 147.5 | 12.5 | 32.9 | 30.0 | 71.6 |
| Apr | 98.0 | 54.8 | 147.8 | 72.6 | 2.0 | 17.4 | 19.5 | 47.1 |
| May | 98.4 | 50.8 | 142.2 | 63.7 | −3.7 | 14.3 | 16.6 | 32.1 |
| June | 97.4 | 37.0 | 380.4 | 106.5 | 12.2 | 42.5 | 15.7 | 34.5 |
| July | 97.8 | 42.4 | 212.8 | 59.1 | 8.6 | 11.3 | 14.7 | 24.4 |
| Aug | 95.4 | 55.6 | 94.1 | 37.2 | −3.5 | 3.6 | 14.0 | 19.8 |
| Sept | 96.6 | 55.8 | 90.8 | 35.2 | −1.6 | 2.9 | 13.3 | 19.7 |
| Oct | 96.6 | 48.8 | 123.8 | 41.6 | −5.6 | 0.7 | 13.0 | 17.4 |
| Nov | 97.8 | 36.6 | 373.4 | 71.2 | 28.7 | 14.4 | 17.7 | 19.8 |

Table 4. Performance on the nowcast date for function $h_2(t)$: **LPS-NB**—LPS model with a negative binomial distribution for the number of cases; **LPS-P**—LPS with a Poisson distribution for the number of cases.

| | 95% PI coverage | | PI width | | Bias (μ) | | % Bias (μ) | |
|-------|-----------------|-------|----------|-------|----------------|-------|------------------|-------|
| | LPS-NB | LPS-P | LPS-NB | LPS-P | LPS-NB | LPS-P | LPS-NB | LPS-P |
| March | 95.0 | 63.4 | 115.3 | 57.5 | 6.1 | 8.8 | 35.6 | 52.2 |
| Apr | 96.8 | 62.4 | 67.6 | 34.9 | −0.3 | 4.1 | 20.0 | 32.9 |
| May | 97.6 | 53.8 | 103.6 | 45.6 | −2.3 | 7.9 | 16.2 | 27.7 |
| June | 98.0 | 44.4 | 178.6 | 62.0 | −1.1 | 16.8 | 14.0 | 28.3 |
| July | 97.0 | 43.8 | 184.6 | 56.6 | 2.2 | 12.6 | 13.5 | 24.0 |
| Aug | 97.2 | 49.0 | 129.2 | 45.0 | −2.4 | 7.9 | 13.0 | 21.4 |
| Sept | 95.8 | 44.4 | 136.3 | 45.5 | −4.6 | 6.2 | 12.5 | 20.4 |
| Oct | 97.6 | 38.2 | 257.7 | 63.0 | −0.7 | 10.5 | 11.5 | 20.4 |
| Nov | 97.2 | 29.4 | 455.9 | 81.7 | 21.2 | 17.6 | 12.8 | 20.6 |

**Figure 4.** COVID-19 death (a) and incidence (b) cases in Belgium. Dashed vertical lines correspond to selected nowcast dates.

prediction interval (PI) coverage and prediction interval width to measure the predictive accuracy of our methodology. For a given calendar day t , the bias and relative bias are computed as $\text{Bias}_t = (1/S) \sum_{s=1}^S (\hat{\mu}_{st} - \mu_t)$ and $\% \text{Bias}_t = (1/S) \sum_{s=1}^S |(\hat{\mu}_{st} - \mu_t) / \mu_t| \times 100\%$, respectively, where $S = 500$ is the number of simulations, μ_t is the target value for the mean epidemic curve and $\hat{\mu}_{st}$ is the corresponding mean nowcast estimate at time t and simulation s . The prediction interval coverage is obtained by determining the percentage of (true) unreported cases that fall within the computed interval. Moreover, for each simulation, the interval width is obtained, that is, the difference between the upper and lower bound of the prediction interval.

The nowcast date is fixed at the end of the month (from March to November). For each nowcast date, the prediction performance is computed for the dates having unreported cases, that is, for $t = T - (D - 1), \dots, T$. As we fixed a maximum delay of 7 days, there will be seven dates (including the nowcast date) that involve the prediction of unreported cases. Here, we

only report simulation results on the nowcast day, that is, at time T . Tables 1–4 summarize the results of the prediction performance on the nowcast date for the different functions being considered.

In terms of prediction interval, the Poisson model with LPS generally exhibits the smallest prediction interval widths resulting in lower coverage rates for all functions. This is expected since data are simulated from the negative binomial distribution which has an overdispersion feature that is not accounted for by the Poisson distribution. For function $f_1(t)$ (Table 1), LPS-NB has more stable coverage rates and is closer to the nominal 95% prediction interval across all nowcast dates compared to VDK. The method of VDK on the other hand, tends to overcover due to wider prediction intervals, indicating higher uncertainty in its predictions. For functions $h_1(t)$ (Table 2) the PI coverage for LPS-NB and VDK are somewhat similar. The PI width of LPS-NB are larger from March to June and smaller from July to November compared to VDK.

Table 5. Proportion of cases reported for each delay in the mortality data.

| Delay (days) | 0 | 1 | 2 | 3 | 4 | 5 | 6 | 7 |
|--------------|-------|-------|-------|-------|-------|-------|-------|-------|
| Proportion | 0.000 | 0.143 | 0.664 | 0.118 | 0.047 | 0.017 | 0.007 | 0.004 |

Table 6. Proportion of cases reported for each delay in the incidence data.

| Delay (days) | 0 | 1 | 2 | 3 | 4 | 5 | 6 | 7 |
|--------------|-------|-------|------|-------|-------|-------|-------|-------|
| Proportion | 0.000 | 0.001 | 0.61 | 0.373 | 0.012 | 0.002 | 0.001 | 0.001 |

The bias of the three methods varies across functions and months. LPS-NB and LPS-P often exhibit similar bias patterns, while VDK occasionally shows higher biases, particularly for function $f_1(t)$ during months like July and November. However, the biases are relatively small in magnitude. In terms of relative bias, VDK sometimes displays higher values compared to LPS-NB and LPS-P, especially noticeable in function $f_1(t)$ during months like July and November. For functions $f_2(t)$ and $h_2(t)$ (Tables 3 and 4) with relatively high case numbers, we did not present the method of Van de Kastele, Eilers, and Wallinga (2019) since their results yield excessively wide prediction intervals and large relative bias. We believe that the reason for this is more of a computational issue rather than a methodological one. The LPS-NB model for these functions yield stable results with higher coverage rates, wider PI, lower relative bias and generally lower bias compared to the LPS-P model.

4. Real Data Application

The proposed nowcasting method is applied to COVID-19 mortality data in Belgium for 2021 and incidence data for 2022. Raw data was downloaded from the website of the Sciensano research institute (<https://epistat.sciensano.be/covid/>; Accessed December 20, 2022). The data contains the cumulative number of cases, reported up to the day of the file. The file is updated every day, and in this way, the number of cases and reporting delays are available. Data is structured in matrix format with the date of death/confirmed case as rows and number of days of reporting delay as columns. Figure 4 shows the total number of cases with (dashed) vertical lines corresponding to different nowcast dates used for illustration. As no cases are reported immediately on the day of death/confirmed case in the data, all cases have a delay of at least one day. The proportion of cases reported for each delay is shown in Table 5. Most of the cases (66% for mortality and 61% for incidence) are reported with a delay of 2 days, followed by a delay of 1 day (14%) for mortality and 3 days (37%) for incidence. The rest of the delays account for a very small percentage of the cases. The reporting delay is truncated to a maximum number of seven days.

We choose $K_T = 40$ and $K_D = 10$ for the real data analysis. In addition, we consider the day of the week effect as an additional covariate in the model. Specifically, we fit the following model $\log(\mu_{t,d}) = \beta_0 + \sum_{j=1}^{K_T} \sum_{k=1}^{K_D} \theta_{j,k} b_j(t) b_k(d) + \sum_{l=1}^6 \beta_l z_l(t, d)$ as in (2.1), where $\sum_{l=1}^6 \beta_l z_l(t, d)$ represents the day of the week with Monday taken as the reference category. Algorithms to fit the model are available in the EpiLPS package (Gressani 2021) through the `nowcasting()` routine.

Figure 5 presents the observed (reported and not-yet-reported) cases for the past 14 days and nowcasting results using the mortality data at different nowcast dates (last day of each month). The blue color represents the confirmed cases that are already reported as of the nowcast date. The gray color represents the observed cases that have not yet been reported as of the nowcast date. The red points with error bars correspond to the nowcast prediction, with a 95% prediction interval. It can be seen that most of the nowcast predictions on the nowcast date are fairly close to the observed not-yet-reported cases (gray). In addition, all of the observed cases fall within the prediction interval. For the incidence data, we used a maximum delay of 5 days. The nowcast results for the incidence data (Figure 6) tend to exhibit varying degrees of accuracy. This means that some nowcast values are close to the observed values, while others are further away, and some are moderately close. Notably, the nowcast estimates (on the nowcast day) for May and July are more distant from the observed values.

The estimated delay density is shown in supplementary material S5. Results show that the delay distribution is fairly stable over time for both incidence and mortality data. The density is highest for a two-day delay except in the beginning of the year for incidence data. This confirms the observed reporting intensity in our data as most cases are reported with a two-day delay.

5. Conclusion

We propose a fast and flexible Bayesian approach for nowcasting based on the framework of Van de Kastele, Eilers, and Wallinga (2019) by coupling P-splines and Laplace approximations. Based on the results presented in this article, Bayesian nowcasting with Laplacian-P-splines seems to be a promising tool. Simulation results demonstrate that our method, under the assumption of a negative binomial distribution, produces stable results with excellent prediction interval coverage and relatively small bias. The nowcast predictions for the mortality data of Belgium seem to be fairly close to the observed not-yet-reported values, and all prediction intervals for the different nowcast dates being considered contain the observed values. For incidence data characterized by a large number of cases, the nowcast results tend to exhibit varying degrees of accuracy. However, it is important to emphasize the absence of data on the nowcast day and that there are very few reported cases (0.1%) with a one-day delay for the incidence data. This makes it much more difficult to produce accurate nowcast predictions.

While nowcasting can provide valuable real-time information and predictions, it also has certain drawbacks. Nowcast-

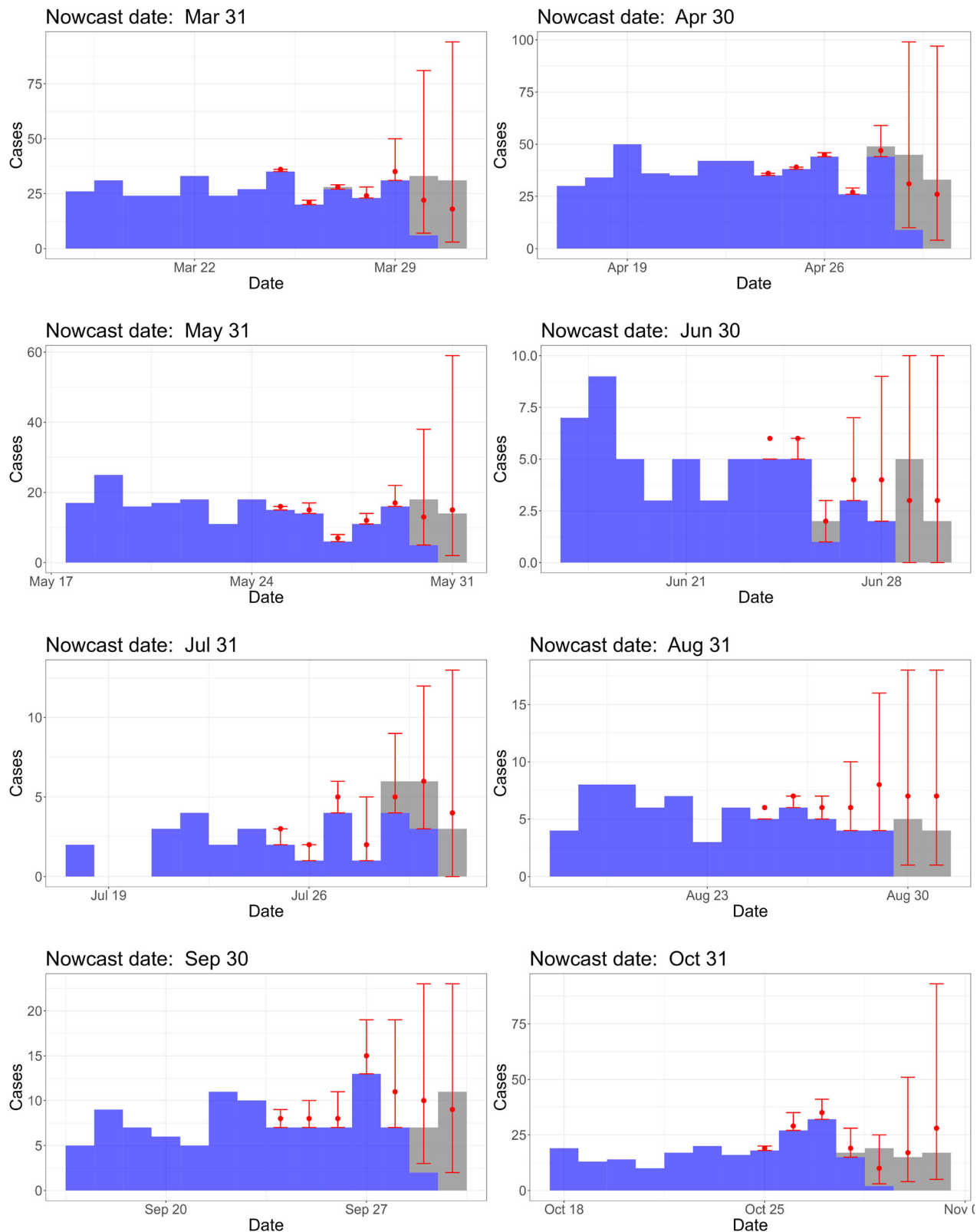


Figure 5. Nowcast for mortality data with different nowcast dates. Blue—reported cases ; Gray—not-yet-reported cases; Red points—nowcast estimates; Red error bar—95% nowcast prediction interval.

ing heavily relies on real-time data, which may not always be readily available or of good quality. Biases in the data (such as double-counting of cases) that are corrected at a later time can impact the nowcasting prediction. In addition, gaps in data collection, processing, or dissemination can impact the

timeliness and effectiveness of nowcasting predictions. Despite these drawbacks, nowcasting has been a very important tool for obtaining timely information and short-term predictions. While the proposed nowcasting model is rather complex, we have embedded the *nowcasting()* routine in the EpiLPS pack-

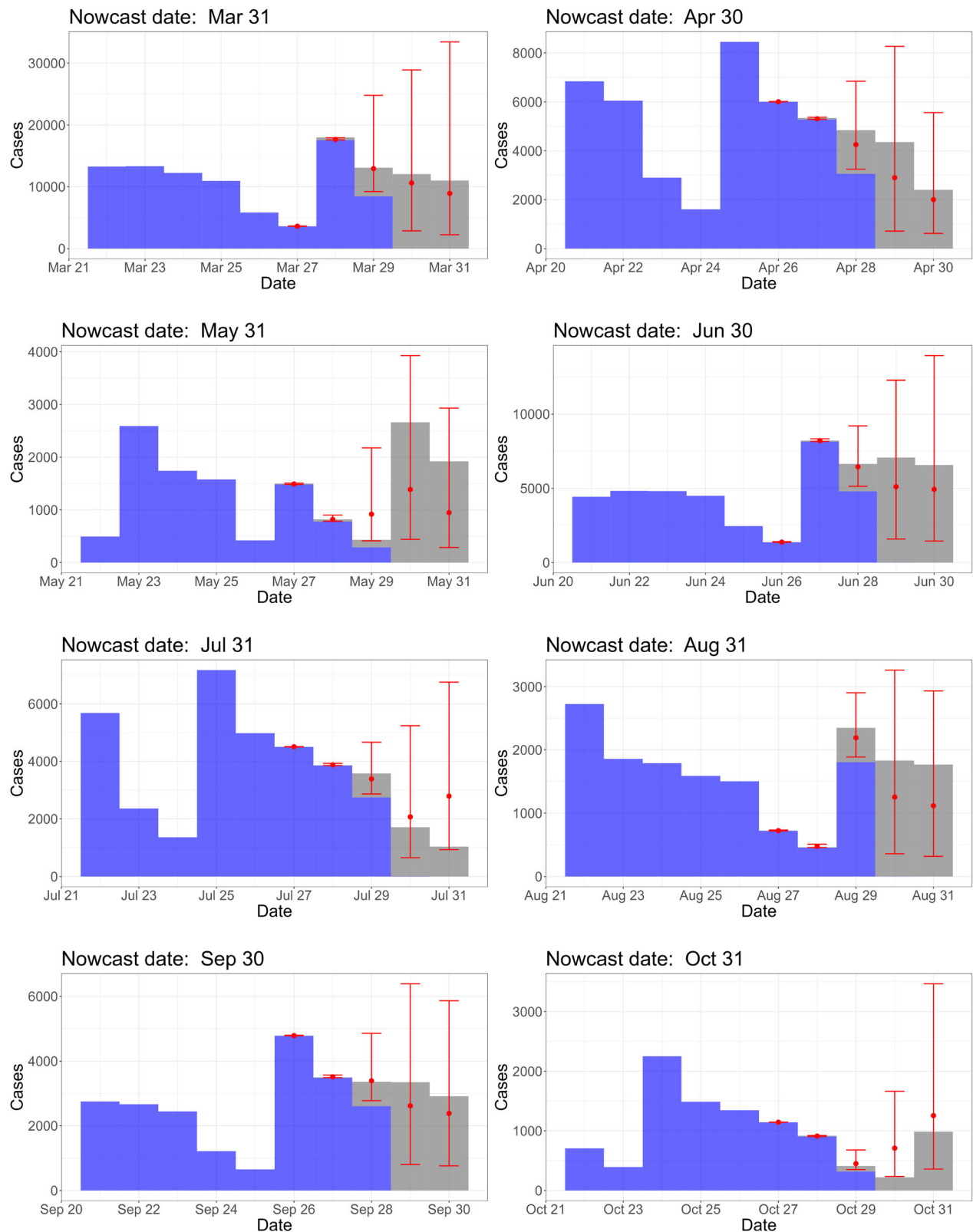


Figure 6. Nowcast for incidence data with different nowcast dates. Blue—reported cases ; Gray—not-yet-reported cases; Red points—nowcast estimates; Red error bar—95% nowcast prediction interval.

age (Gressani 2021) to provide a user-friendly experience. An interesting extension of the LPS nowcasting approach is to include it within a model for the time-varying reproduction number (Gressani et al. 2022b) as recently proposed by Sumalinab et al. (2024). Another possible extension is to consider

the correlation of cases for each time point t . By doing this, the model will be able to capture temporal dependencies and may provide better estimates of variability. Finally, accounting for spatial correlation and other covariate effects would be valuable.

Supplementary Materials

Online Appendix: Contains details for the model matrices and parameters, derivations for the gradient and Hessian, hyperparameter optimization, details for the LPS-Poisson model, supplementary figures, and tables.

R scripts: R code used to implement the simulation study is available on GitHub (<https://github.com/bryansumalinab/Laplacian-P-spline-nowcasting.git>).

Disclosure Statement

The authors have declared no competing interest.

Funding

VERDI: This project was supported by the VERDI project (101045989), funded by the European Union. Views and opinions expressed are however those of the author(s) only and do not necessarily reflect those of the European Union or the Health and Digital Executive Agency. Neither the European Union nor the granting authority can be held responsible for them.

ESCAPE: This project was supported by the ESCAPE project (101095619), funded by the European Union. Views and opinions expressed are however those of the author(s) only and do not necessarily reflect those of the European Union or European Health and Digital Executive Agency (HADEA). Neither the European Union nor the granting authority can be held responsible for them.

The authors acknowledge funding from the Special Research Fund through the Methusalem project BOF22M01.

ORCID

Bryan Sumalinab  <http://orcid.org/0000-0001-8264-5336>

References

- De Angelis, D., and Gilks, W. (1994), "Estimating Acquired Immune Deficiency Syndrome Incidence Accounting for Reporting Delay," *Journal of the Royal Statistical Society, Series A*, 157, 31–40. [718]
- Donker, T., van Boven, M., van Ballegooijen, W. M., van't Klooster, T. M., Wielders, C. C., and Wallinga, J. (2011), "Nowcasting Pandemic Influenza A/H1N1 2009 Hospitalizations in the Netherlands," *European Journal of Epidemiology*, 26, 195–201. [718]
- Durbán, M., Currie, I., and Eilers, P. H. C. (2002), "Using P-Splines to Smooth Two-Dimensional Poisson Data," in *Proceedings of 17th International Workshop on Statistical Modelling*, Chania, Crete, pp. 207–214. [719]
- Eilers, P. H. C., and Marx, B. D. (1996), "Flexible Smoothing with B-splines and Penalties," *Statistical Science*, 11, 89–121. [718,719]
- Fahrmeir, L., Kneib, T., Lang, S., and Marx, B. (2013), *Regression: Models, Methods and Applications*, Berlin: Springer. [719]
- Glöckner, S., Krause, G., and Höhle, M. (2020), "Now-Casting the COVID-19 Epidemic: The Use Case of Japan, March 2020," medRxiv. [718]
- Gressani, O. (2021), *EpiLPS: A Fast and Flexible Bayesian Tool for Estimating Epidemiological Parameters*, [Computer Software]. <https://epilps.com/>. [725,727]
- Gressani, O., Faes, C., and Hens, N. (2022a), "Laplacian-P-Splines for Bayesian Inference in the Mixture Cure Model," *Statistics in Medicine*, 41, 2602–2626. [719]
- (2023), "An Approximate Bayesian Approach for Estimation of the Instantaneous Reproduction Number Under Misreported Epidemic Data," *Biometrical Journal*, 65, 2200024. [719]
- Gressani, O., and Lambert, P. (2018), "Fast Bayesian Inference Using Laplace Approximations in a Flexible Promotion Time Cure Model based on P-splines," *Computational Statistics & Data Analysis*, 124, 151–167. [719]
- (2021), "Laplace Approximations for Fast Bayesian Inference in Generalized Additive Models based on P-splines," *Computational Statistics & Data Analysis*, 154, 107088. [719]
- Gressani, O., Wallinga, J., Althaus, C. L., Hens, N., and Faes, C. (2022b), "EpiLPS: A Fast and Flexible Bayesian Tool for Estimation of the Time-Varying Reproduction Number," *PLoS Computational Biology*, 18, e1010618. [719,727]
- Günther, F., Bender, A., Katz, K., Küchenhoff, H., and Höhle, M. (2021), "Nowcasting the COVID-19 Pandemic in Bavaria," *Biometrical Journal*, 63, 490–502. [718]
- Gutierrez, E., Rubli, A., and Tavares, T. (2020), "Delays in Death Reports and their Implications for Tracking the Evolution of COVID-19," available at SSRN 3645304. [718]
- Höhle, M., and an der Heiden, M. (2014), "Bayesian Nowcasting During the STEC O104: H4 Outbreak in Germany, 2011," *Biometrics*, 70, 993–1002. [718]
- Jullion, A., and Lambert, P. (2007), "Robust Specification of the Roughness Penalty Prior Distribution in Spatially Adaptive Bayesian P-Splines Models," *Computational Statistics & Data Analysis*, 51, 2542–2558. [720]
- Lambert, P., and Gressani, O. (2023), "Penalty Parameter Selection and Asymmetry Corrections to Laplace Approximations in Bayesian P-Splines Models," *Statistical Modelling*, 23, 409–423. [720]
- Lang, S., and Brezger, A. (2004), "Bayesian P-splines," *Journal of Computational and Graphical Statistics*, 13, 183–212. [718,719]
- Lawless, J. (1994), "Adjustments for Reporting Delays and the Prediction of Occurred but not Reported Events," *Canadian Journal of Statistics*, 22, 15–31. [718]
- Lindsey, J. (1996), "Fitting Bivariate Intensity Functions, with an Application to Modelling Delays in Reporting Acquired Immune Deficiency Syndrome," *Journal of the Royal Statistical Society, Series A*, 159, 125–131. [718]
- Noufaily, A., Farrington, P., Garthwaite, P., Enki, D. G., Andrews, N., and Charlett, A. (2016), "Detection of Infectious Disease Outbreaks from Laboratory Data with Reporting Delays," *Journal of the American Statistical Association*, 111, 488–499. [721]
- Rue, H., Martino, S., and Chopin, N. (2009), "Approximate Bayesian Inference for Latent Gaussian Models by Using Integrated Nested Laplace Approximations," *Journal of the Royal Statistical Society, Series B*, 71, 319–392. [720]
- Sumalinab, B., Gressani, O., Hens, N., and Faes, C. (2024), "An Efficient Approach to Nowcasting the Time-Varying Reproduction Number," *Epidemiology*, 35, 512–516. [719,727]
- Van de Kasstele, J., Eilers, P. H. C., and Wallinga, J. (2019), "Nowcasting the Number of New Symptomatic Cases During Infectious Disease Outbreaks Using Constrained P-Spline Smoothing," *Epidemiology*, 30, 737–745. [718,719,721,723,725]